Low Spatio-Temporal Frequency Wavefront Aberration Correction Method Based on a Movable Secondary Mirror

Yawei Xiao, Simin Zhao, Junbo Zhang, Linhai Huang, and Naiting Gu

***Abstract*—A low frequency wavefront aberration correction method for solar telescopes based on secondary mirror movement is proposed to correct dynamic wavefront aberration during the operation of solar telescope. The correction ability of this method is analyzed and validated by numerical simulation and experiments. Theoretical analysis and numerical simulation both indicate the system processes significant aberration correction ability given the correction frequency of the secondary mirror movement is 10 times higher than aberration frequency. After spatiotemporal frequency division of actual wavefront data from solar telescope, the experiment result proves that the proposed correction method based on secondary mirror movement can effectively reduce the overall RMS of dynamic aberrations with high-frequency portion.**

***Index Terms*—Imaging system, aberration correction, secondary mirror, sensitivity matrix method, solar telescope.**

I. Introduction

THE imaging quality and resolution of large aperture solar telescope system is limited by various influence factors, such as optical and mechanical structure deformation from solar radiation, gravity bending, and environmental temperature fluctuation [1], [2], etc. These influencing factors are introducing aberrations with similar frequency characteristics during observation. Based on the frequency characteristics, these aberrations are generally been categorized as low-order and low-frequency aberration, also known as low space-time frequency wavefront aberration.

In practice, there also exist high frequency aberrations arise from wind borne and atmospheric turbulence. During observation, the aberrations containing all frequency bands are mixed together and downgrade the regular observation result of optical system. At present, all of the above aberrations are been detected and corrected by Adaptive Optics (AO) system.

If the low frequency portion of aberrations can be corrected by other pre-processing methods, then let the Adaptive Optics system focus on high frequency aberrations only, fully release its potential, and achieve better correction result. In general, low frequency aberrations come from various degrees of deflection and skewing of optical axis with respect to pitch angle changes during observation. Meanwhile, the fluctuation of environmental temperature also contributes to the deformation of telescope main tube and mirror, resulting in low frequency aberrations. This is a common problem for solar telescopes, and cannot be solved by pre-assemble and adjustment in integration and adjustment stages.

In order to correct low frequency aberrations during observation, the method of secondary mirror movement have been widely used. This method controls the adjustment of position and orientation of secondary mirror. At present, there are two main types of method's working modes, the open loop mode and closed loop mode.

The principle of open-loop working mode is to estimate the position relationship between the primary and secondary mirror under different pitch angles according to the telescope structure model, and compensate the misalignment with respect to each pitch angle during operation. This method is adopted by the 2 m ground based optical telescope of the Changchun Institute of Optics, Fine Mechanics and Physics, CAS [3]. This open-loop working mode system does not require a sensor, and the lookup table established pre-observation achieves a high precision level with repeated calibration. However, the correction target of open-loop system is limited only on the displacement between primary and secondary mirror from bending of the pointing structure. Thus, open-loop system is unable to handle aberrations from sources other than mechanical bending by secondary mirror movement effectively.

The principle of close loop working mode is to control the position of the secondary mirror through feedback information. The feedback information includes the position relationship of the primary and secondary mirror measured by a laser tracker, for example the LBT telescope [4] in the United States. In other practice, the close loop feedback information could also be the average aberration value from Shaker Hartmann wavefront

Manuscript received 18 November 2023; revised 8 March 2024; accepted 22 March 2024. Date of publication 27 March 2024; date of current version 19 April 2024. This work was supported in part by the National Natural Science Foundation of China (NSFC) under Grant 12293031, Grant 12022308, and Grant 12073031, in part by The National Key R&D Program of China under Grant 2021YFC2202204 and Grant 2021YFC2202200, and in part by The distinguished Youth Innovation Promotion Association, Chinese Academy of Science, under Grant Y2022097. *(Yawei Xiao and Simin Zhao contributed equally to this work.) (Corresponding author: Naiting Gu.)*

The authors are with the Institute of Optics and Electronics, Chinese Academy of Sciences, Chengdu 610209, China, also with the The Key Laboratory on Adaptive Optics, Chinese Academy of Sciences, Chengdu 610209, China, and also with the University of Chinese Academy of Science, Beijing 100049, China (e-mail: yawei524@foxmail.com; aigelaomao@163.com; 244817690@qq.com; hlhjs@163.com; gnt7328@163.com).

Digital Object Identifier 10.1109/JPHOT.2024.3382591

detector. In practice, the Shaker Hartmann wavefront detector records a long period of data to eliminate the high frequency aberration such as atmospheric disturbance and focus on the rest low frequency aberration to calculate the adjustment amount of secondary mirror, for example the LSST [5], German GREGOR [6], GST [7] and DKIST [8] in United States, 2m telescope [9] in China. The LSST telescope is equipped with active optics system operating at 0.025 Hz. GREGOR is equipped with a tilting mirror to adjust the misalignment of telescope optics and keep pupil image at the center of wavefront sensor. Comparing with open loop mode, the closed loop mode releases the full potential of low order aberration correction of the secondary mirror movement.

However, current close loop working mode cannot effectively utilize the dynamic ability of the secondary mirror adjustment mechanism to achieve real-time dynamic aberrations correction such as aberrations from atmospheric disturbance and wind-borne structural deformation. If we can make fully use of the secondary mirror adjusting mechanism such as travel range and dynamic capability, and process the aberrations based on wavefront sensor frequency data, effective correction of low spatio-temporal frequency aberrations of secondary mirror can be realized and the imaging resolution of solar telescope system can be further improved.

Based on aforementioned background, this paper takes the POST solar telescope [10] as research object and studied the dynamic low spatio-temporal frequency wavefront aberration correction method based on secondary mirror movement. First, basic parameters of the telescope and the correction mechanism of secondary mirror movement targeting aberration correction is introduced. Then, numerical calculations and simulation of correction effectiveness were performed on various dynamic aberration frequencies introduced by gravity deflection and thermal deformation of telescope structure. Then, the correction effectiveness on various frequency aberrations by secondary mirror adjustment is analyzed in detail, and experiment were performed to verify the necessity of spatio-temporal frequency division process for mixing frequencies dynamic aberrations correction. In conclusion, simulation and experiment results both show that the rigid body movement of secondary mirror processes a remarkable correction effect on aberrations of low spatio-temporal frequency of solar telescope. With further increase of dynamic adjustment frequency of the secondary mirror, the correction of higher frequencies aberrations will be achieved.

II. Telescope Optical System

The POST Solar Telescope was designed and built between 2014 and 2017 to validate and solve some of the technical and engineering challenges of the CLST [11] solar telescope. The POST solar telescope adopts an axially symmetric Gregorian system. Its optical layout and schematic are shown in Fig. 1 and system parameters are shown in Table I.

Generally, the orientation and position of secondary mirror of symmetrical telescope is controlled by rotation around the X/Y axis (where Z axis is the optical axis in Cartesian coordinates) and displacement in three dimensions. The wavefront aberrations are mainly consisting of oblique aberration, defocusing aberration, coma, minor spherical aberration, astigmatism etc [12], [13], [14]. Among all of the aberrations above, aberrations caused by system misalignment such as structural deformations and bending, can be corrected by adjusting the position and orientation of the secondary mirror. For non-misalignment aberrations caused by thermal deformation of mirror, ambient temperature fluctuation, atmospheric disturbance, etc., which include tilt, defocusing, coma, spherical and astigmatism. Among which the tilt and defocus aberrations processes similar characters of misalignment aberrations, and thus can be corrected effectively by secondary mirror movement. The rest other aberrations such as coma, spherical, astigmatism also process some characteristics of position mismatch, but they exist in a combination of certain ratio, and thus the secondary mirror movement can only partially correct them as a whole [15].

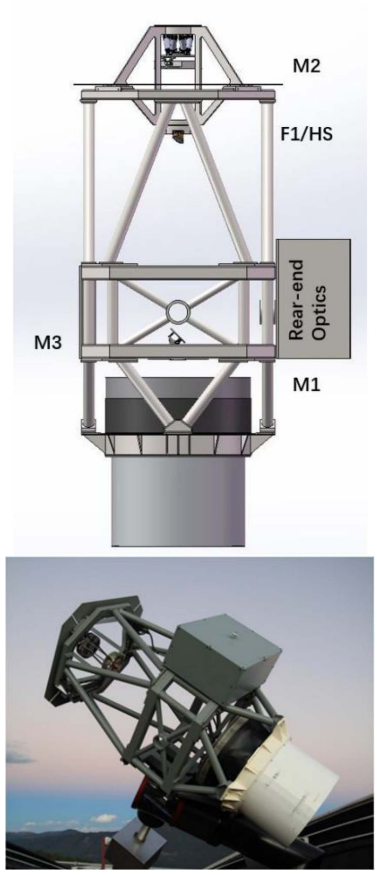

Fig. 1. Optical layout of POST (a) and the telescope (b).

TABLE I
Specifications of POST Solar Telescope

Surface	Mechanical diameter / d/mm	Radius of curvature r/mm	Interval D/mm	Conic factor
Primary mirror	600	-2040	-1320	-1
Secondary mirror	180	504.812	—	-0.466

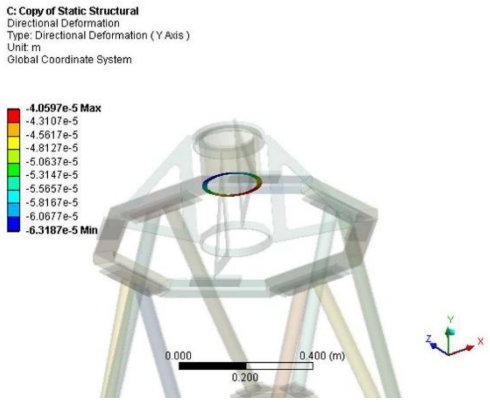

Fig. 2. Deformation of secondary mirror fixing surface when the main tube in zenith state.

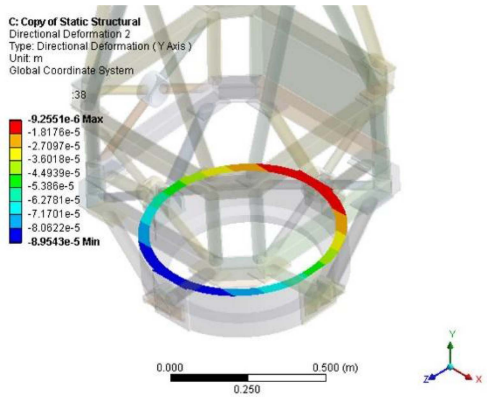

Fig. 3. Deformation of primary mirror tube when the main tube in zenith state.

While moving the secondary mirror in the direction of 5 degrees of freedom, a numerical relationship between the displacement of secondary mirror and aberration correction results can be established. We adopt second-order sensitivity matrix [16], [17] as the fundamental method in this paper to establish this relationship, as shown in (1). In practice, the adjustment amount of secondary mirror is calculated based on sensitivity matrix, and then executed by Hexapod. That's working mode of real-time correction of the low space-time frequency of the telescope.

$$Z - Z_0 = A\Delta \mathrm{X}.^2 + B\Delta \mathrm{X} + \delta \tag{1}$$

Where, Z and Zo is the Zernike coefficient at current position and initial position repectively, A and B represents the quadratic term coefficient matrix and the primary term coefficient matrix, respectively. ΔX represents the displacement of the secondary mirror along the direction of each degree of freedom, $\Delta \mathrm{X}.^2$ represents the matrix formed by the square of the displacement of the secondary mirror in the direction of each degree of freedom, and δ is the residual error.

III. The Analysis of Low Spatio-Temporal Aberration of Solar Telescope

There are many sources of low spatio-temporal frequency wavefront aberrations in regular observation process of solar telescope. Restricted by load, precision requirements and engineering ability, the highest dynamic frequency of POST Hexapod is 0.5 Hz. The effectiveness of rigid body secondary mirror correction under current conditions can be analyzed by spatio-temporal characteristics of these aberrations and propose dynamic frequency requirements for Hexapod system.

Because of the change in pitch angle during operation of telescope, the support structure of the primary and secondary mirrors is affected by the change in relative angle between pointing axis and gravity, which leads to different degrees of bending, eccentricity and tilt between the primary and secondary mirrors, as shown in Figs. 2 and 3. When the main tube in zenith state, the primary and secondary mirror spacing shifts 49μm along the gravity direction. Whereas in the case of main tube in horizontal state, the primary and secondary mirror intervals are offset by 9.5μm along the optical axis and 46μm along the gravity direction, as a result, the relative tilt of primary and secondary mirrors is 7.5".

TABLE II
Zernike Orders With Associated Aberration

Zernike Order	Aberration
Z1	Piston
Z2	Tip
Z3	Tilt
Z4	Defocus
Z5	Astigmatism
Z6	Astigmatism
Z7	Coma
Z8	Coma

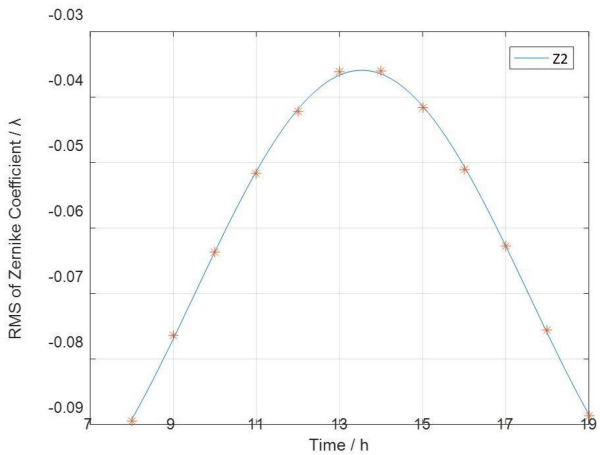

Fig. 4. Changes of oblique aberration during a day's observation from structure bending.

Through the simulation of aberrations from misalignment between the primary and secondary mirrors at different pitch angles throughout a whole day, we obtain the aberration result over time of POST solar telescope continuously tracking the sun. The changes of oblique aberrations and defocusing aberrations are shown in Figs. 4 and 5 respectively. This paper adopts the

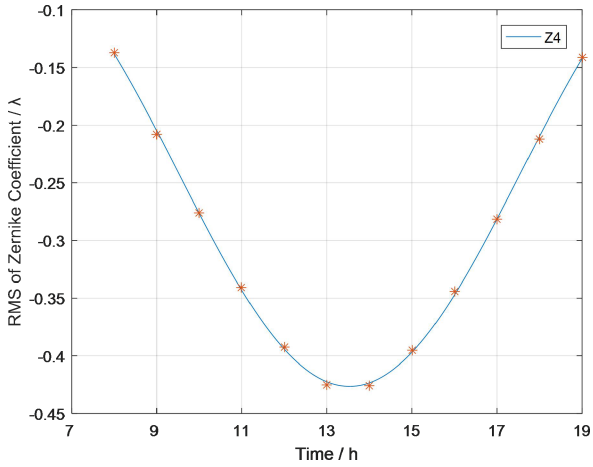

Fig. 5. Changes of defocusing aberration during a day's observation from structure bending.

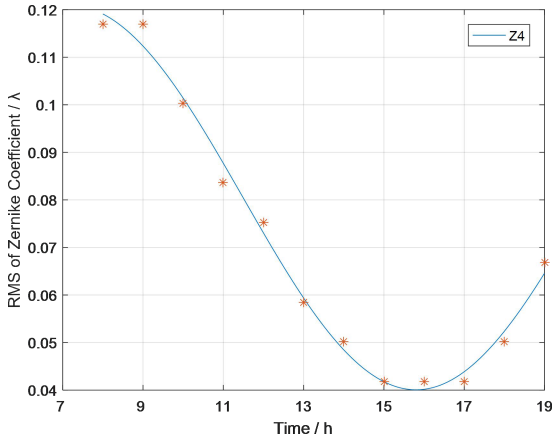

Fig. 7. Changes of defocusing aberration during a day's observation from thermal deformation.

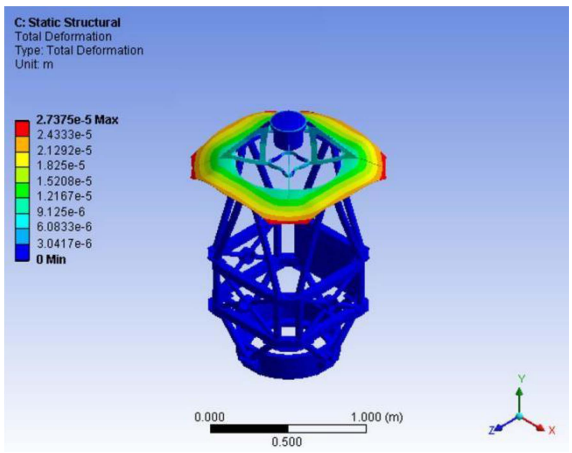

Fig. 6. Thermal deformation of main tube.

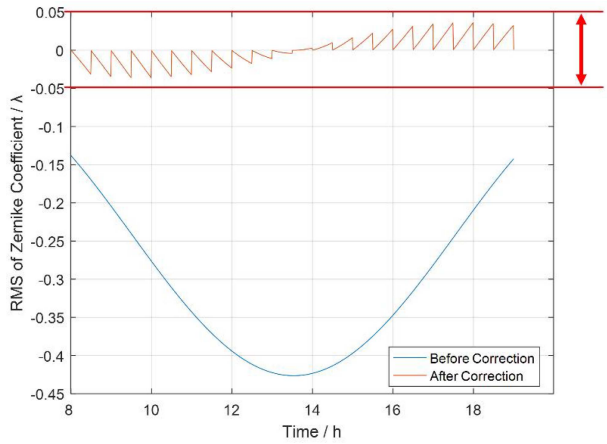

Fig. 8. Correction of defocusing aberration from structure bending by secondary mirror rigid body displacement.

standard Zernike orders shown in Table II, [18] starting from Z1, which represents piston, Z2 and Z3 represents tip and tilt, Z4 represents defocus, Z5 and Z6 represents astigmatism, Z7 and Z8 represents coma, etc.

Apparently, due to thermal radiation from the sun, there is a significant surface temperature gap of solar telescope between the sun side and back side. Because of solar radiation and ambient temperature fluctuation, there is a structural deformation that leads to misalignment between the primary and secondary mirror, which mainly leads to defocus aberration. Given ambient temperature of 22 degree Celsius and solar telescope pointing to zenith position under maximum solar radiation, the maximum deformation of the main tube is 12 μm, as shown in Fig. 6. According to the environmental temperature data of a specific day in winter at the telescope site, the changes of defocusing aberration with time under the influence of temperature and solar radiation can been simulated, as shown in Fig. 7.

The frequency range of the above aberrations is analyzed, with a result of dynamic frequencies all lower than $2x10^{-5}$Hz. For example, the defocusing aberration from structural bending only requires for an adjustment frequency of 0.005 Hz. After correction, the maximum defocusing aberration RMS is lower than 0.05λ and result is shown in Fig. 8. The adjustment frequency of 0.005 Hz is much lower than Hexapod adjustment frequency, which proves that the current Hexapod adjustment frequency meets the requirements for low space-time frequency aberration correction of solar telescope.

In practice, there are a number of low spatio-temporal frequency aberrations from wind load and atmospheric turbulence. Take the tilt power spectrum recorded by X. Li as example, there consists of a large portion of low frequency signal, specifically under 0.5 Hz [19].

In addition to literature, the spatial frequencies of the candidate wavefront were analyzed by Zemax software. From simulation, the spatial frequency aberration mainly comes from the displacement of secondary mirror, including sources of structural deformation from gravity, position mismatch, etc. In experiment, several representative static and dynamic Zernike aberrations were selected to test the effectiveness of the correction system, which can cover the temporal and spatial frequency of the practical POST.

Based on the frequency domain data, rigid body displacement of secondary mirror adjustment mechanism is capable of correcting these types of low frequency aberrations. However, the high and low frequencies aberration signal always exits together and high frequency signal affects the processing of low frequency signal. For example, the processing of all frequency aberrations could result in signal amplification rather than contraction instead. Thus, a frequency separation is required to divide the aberration based on its frequency domain, and focusing on correcting low frequency signal to realize the adjustment of low frequency aberration correction.

IV. The Dynamic Aberration Correction Based on Hexapod

To achieve dynamic correction for low spatio-temporal frequency aberrations, secondary mirror demands for a dynamic platform that can adjust at higher frequencies in five degrees of freedom. Hexapod platform has been widely used as a secondary mirror adjustment platform for large photoelectric telescopes for advantages such as precision control, structural rigidity, high load capacity, system stability, and no position accumulation errors, etc [20]. The Hexapod of POST Solar telescope comes with a highest adjustment frequency of 0.5 Hz, which is taken as the frequency of aberration correction. Besides part of the simulation frequencies is very low, to validate the proposed method stricter, and push the system to its fully potential, various aberrations at different frequencies are simulated and analyzed.

A. Simulation of Single Frequency Dynamic Aberration Correction

Generally, when the sampling frequency is more than twice higher the signal frequency, the sampled digital signal completely retains the information of the original signal. In practice, sampling frequency is usually 2.56 ~ 4 times of signal frequency [21]. Among all aberrations, the tilt and defocusing aberrations are most sensitive to the position and orientation of secondary mirror and can be fully corrected. Taking defocusing aberration as the correction object, and set the secondary mirror correction frequency at 0.5 Hz. Correction simulation is performed for dynamic defocusing aberration of 0.25 Hz, 0.125 Hz, 0.1 Hz, 0.05 Hz and 0.025 Hz (from 1/2 to 1/20 of correction frequency) respectively. The average aberration RMS and PV in a correction cycle is used to represent the correction effectiveness of dynamic secondary mirror rigid body displacement. Correction result of the above aberrations of different frequencies is shown in 3 and Table IV, and the correction result of 0.05 Hz aberration is shown in Fig. 9, Table III. In Fig. 9, the correction frequency is 0.25 Hz, with current aberration value as the target of correction at the beginning of each correction cycle.

The dynamic aberration correction results of fixed frequency are also analyzed. It can be concluded that the higher the frequency ratio of secondary mirror versus aberration, the better the correction results. When the correction frequency is 10 times higher than aberration frequency, the average aberration RMS is 33% and PV is 59% of before. However, when the correction frequency is only less than twice of the aberration

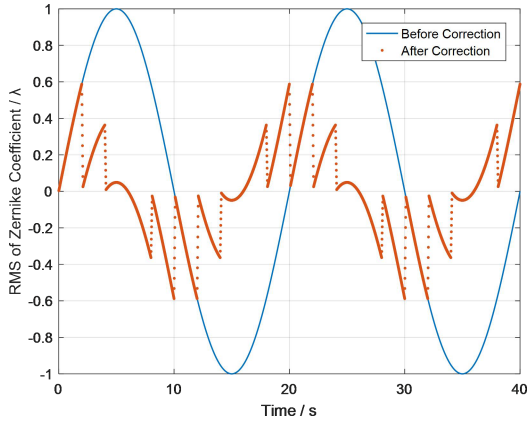

Fig. 9. Aberrations correction of frequency 0.05 Hz.

TABLE III
Results Comparison of Aberrations Correction of Single Frequency

Frequency/Hz	Before Correction RMS Average / λ	After Correction RMS Average / λ	Percentage
0.025	0.6366	0.1051	16.5%
0.05	0.6366	0.2064	32.4%
0.1	0.6366	0.4066	63.8%
0.125	0.6366	0.5267	82.7%
0.25	0.6366	0.6366	100%

TABLE IV
Results Comparison of Aberrations Correction of Single Frequency

Frequency/Hz	Before Correction PV / λ	After Correction PV / λ	Percentage
0.025	2	0.6180	30.9%
0.05	2	1.1756	58.8%
0.1	2	2.0000	100%
0.125	2	2.1266	106.3%
0.25	2	3.4899	174.5%

frequency, there is little correction effect on aberration, even negative optimization may exist. Therefore, it is necessary to separate the signals with respect to its frequency domain and filter the original mixed signal to avoid high frequency aberration affecting the calculation and correction of aberrations.

B. Simulation of Multiple Frequencies Dynamic Aberration Correction

Based on aforementioned conclusion, the aberration correction of the secondary mirror movement is effective given the frequency of correction is more than twice of aberration. Meanwhile, negative optimization may occur in the case of high frequency aberration correction. However, in practice, aberrations of high frequencies and low frequencies always appear together. Therefore, it is necessary to separate dynamic aberrations based on frequency and focusing on correcting low frequency aberrations.

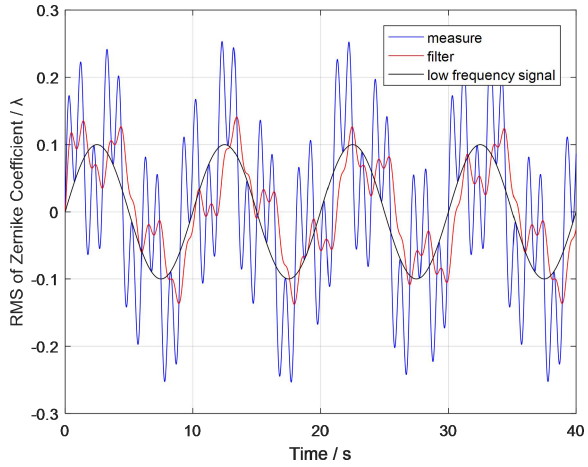

Fig. 10. Filtering effect of Kalman filter for mixed frequency.

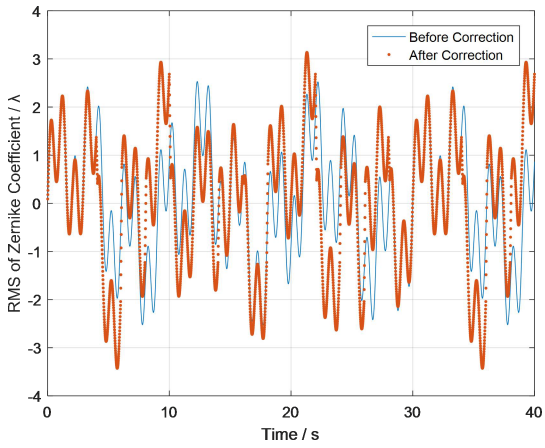

Fig. 11. Correction result without Kalman filter.

Kalman filter [22] is an estimation algorithm based on experience and measurements. The principle of Kalman filter is to make prediction of physical quantities base on comprehensive analysis of previous state and measured value. The signals apart from (1) can be filtered successfully with adequate filtering parameters. The key advantage of Kalman filter is real-time filtering, and that is the reason for us to choose Kalman filter for this application scenario of correcting aberrations. The filtering effect of Kalman filter on dynamic aberrations with multiple frequencies is shown in Fig. 10. Aberration signal can be processed in real time after setting appropriate filtering parameters based on Hexapod correction frequency. The aberration signal obtained after real-time filtering is close to the response of (1) from unprocessed signal. From the results, the aberration signal close to (1) been retained while signals apart from (1) effectively filtered. Thus, Kalman filter meets the requirement of aberration approaching the response of (1) in this paper.

Figs. 11 and 12 shows the correction effectiveness for defocusing aberrations with a large portion of aberration apart from (1) is calculated by aberration data with and without Kalman filtering

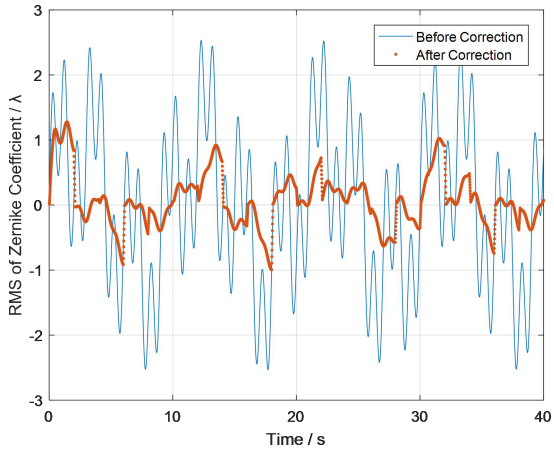

Fig. 12. Correction result with Kalman filter.

TABLE V
COMPARISON OF APPLYING KALMAN FILTER

Filter Applied	Average before correction / λ	Average after correction / λ	Occupation
No	1.0176	1.1859	116.5%
Yes	1.0176	0.3099	30.4%

pre-processing. Table V shows the comparison of aberration correction effect with or without Kalman filtering. After analysis on correction effectiveness, the average aberration RMS is greater than before after correction without Kalman filter. Whereas the average aberration RMS is reduced by 70% with Kalman filter pre-processing to separate the real time aberration signal apart from (1). The component apart from (1) of real-time aberration information can be effectively filtered by Kalman filter and been corrected after secondary mirror correction. When Kalman filter not applied, the system aberration correction even results in negative optimization because of the correction frequency of secondary mirror adjustment mechanism is relatively low compared with high frequency aberration. During the operation of solar telescope, the system aberration is affected by atmospheric turbulence and consists of a large portion of high frequency aberrations, which apart from (1). Therefore, it is necessary to apply Kalman filter to separate the aberration signal approaching (1) and correct them by rigid body displacement of secondary mirror.

C. Experiments of Secondary Mirror Rigid Body Aberration Correction

To verify the correction effectiveness of rigid body displacement of the secondary mirror on low spatio-temporal frequency aberrations, an experiment optical system was set up as shown in Fig. 13. The deformable mirror used in experiment is part of the POST telescope, followed by a reflective mirror and several refractive lenses. The effectiveness and performance before and after moving the secondary deformable mirror is similar with

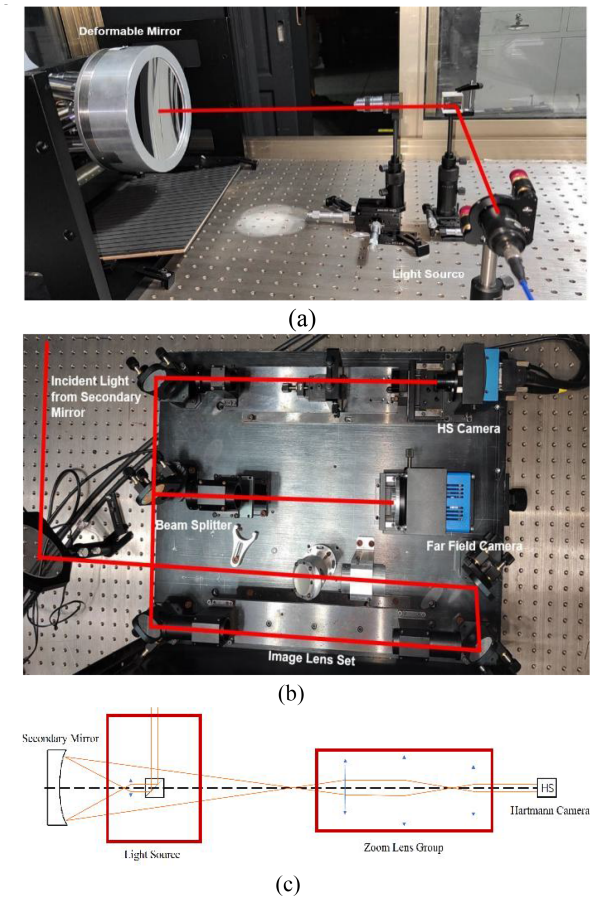

Fig. 13. Experiment set up. (a) The front-end optical instruments, including the light source and deformable secondary mirror. (b) The rear-end optical instruments, including image lens set and HS camera. (c) The schematic of the whole optical layout.

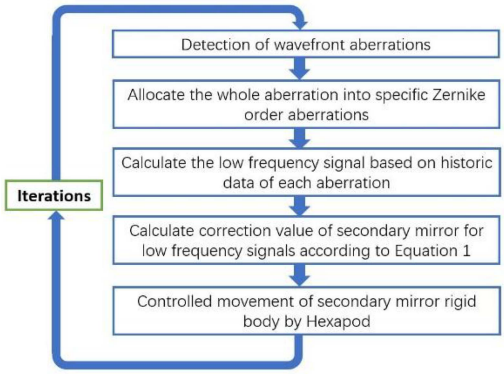

Fig. 14. Flowchart of aberration correction of secondary mirror rigid body displacement.

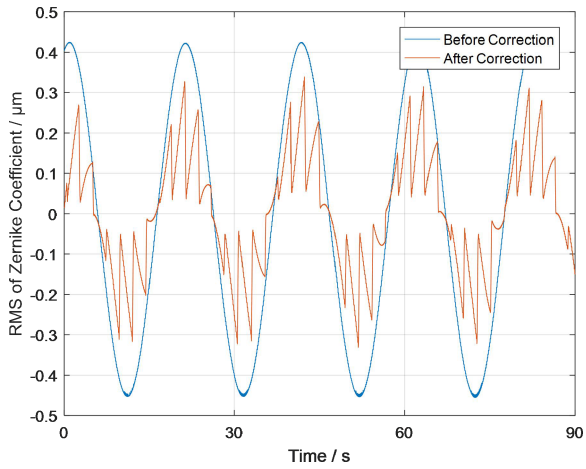

Fig. 15. Defocusing aberration correction at 0.05 Hz.

POST. The primary mirror of POST was simulated by a light source with same focus length, and the position and orientation of secondary mirror is controlled by Hexapod. The deformable secondary mirror was used to generate low spatio-temporal frequency aberration to simulate the actual operation environment of solar telescope. The wavefront aberration of exit pupil plane of the field of view on the axis was measured by Hartmann camera [23]. The software calculating wavefront restoration and solving the value of secondary mirror rigid body displacement correction is developed by Institute of Optics and Electronics, Chinese Academy of Sciences.

The experiment processes are as follows: First, the wavefront slope is detected by Hartmann detector. Then, the whole aberration was processed and allocated into each specific Zernike order of aberration. After that, the system calculates the low frequency signal based on historic data. Zernike polynomial is calculated by algorithm integrated in the software. After that, the secondary mirror step movement amount is calculated using minimum square method and pre-measured sensitivity matrix. Last, Hexapod moves the secondary mirror and correct the low spatio-temporal frequency aberrations. Real time correction was realized through closed-loop iterations with flow chart shown in Fig. 14.

In experiment, dynamic frequency of Hexapod adjusting mechanism of the secondary mirror under load is 0.5 Hz. From simulation result, the correction effectiveness is prominent when the correction frequency of secondary mirror is more than ten times higher than aberration frequency. The secondary mirror has a high correction effect on tilt and defocusing aberrations from sensitivity matrix of secondary mirror and aberration. In experiment, dynamic aberrations including tilt and defocusing are generated by a deformable mirror, and their dynamic frequency is controlled to simulate low spatio-temporal frequency aberrations. The correction results of the secondary mirror of aberrations of tilt and defocusing are shown in Fig. 15.

When correcting multi-order aberrations simultaneously in experiments, the residual defocusing aberration of single correction is about 0.05 μm due to coupling of different degrees of freedom directions and displacement calculation error. But this is the optimal result under current correction frequency. When the aberration frequency is 0.05 Hz, the average of corrected aberration RMS is reduced to 53.7%, PV is reduced to 62% of before, and the frequency of 0.05 Hz is taken as the benchmark of frequency division in this paper. The aberration correction effectiveness of other frequency is shown in Tables VI and VII which

TABLE VI
ABERRATION CORRECTION COMPARISON IN RMS OF SINGLE FREQUENCY

Frequency/ Hz	Before Correction / μm	After Correction / μm	Residual
0.01	0.281	0.035	12.5%
0.025	0.287	0.090	31.4%
0.05	0.281	0.151	53.7%
0.1	0.274	0.266	97.1%
0.25	0.272	0.322	118.3%

TABLE VII
ABERRATION CORRECTION COMPARISON IN PV OF SINGLE FREQUENCY

Frequency/ Hz	Before Correction / μm	After Correction / μm	Residual
0.01	0.494	0.239	48.3%
0.025	0.471	0.342	72.6%
0.05	0.535	0.332	62.0%
0.1	0.319	0.276	86.6%
0.25	0.273	0.281	102.9%

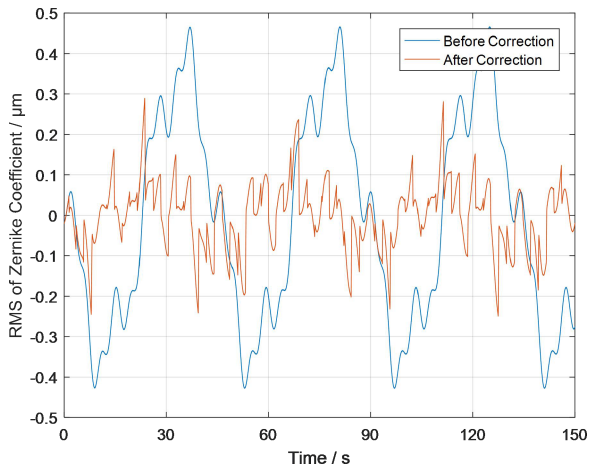

Fig. 16. Aberration correction of mixing frequencies.

further proves the effectiveness of secondary mirror movement for low spatio-temporal frequency aberrations.

In experiment, dynamic aberration of multiple frequencies is generated by a deformable mirror, and the low spatio-temporal frequency aberration is processed by Kalman filtering, then corrected by secondary mirror movement. The correction effectiveness of secondary mirror on defocusing aberration on dynamic aberration of multiple frequencies is shown in Fig. 16.

After correction, dynamic aberration is effectively reduced, with average corrected aberration RMS 35.7%, PV 67.2% of before. After adjusting the frequency composition of aberration and repeated the experiment, the correction results secondary mirror movement are shown in the Tables VIII and IX After correction, the average RMS of each group of mixed aberrations is 40% (PV 30%) lower than before, which verifies the correction effectiveness of secondary mirror movement for mixed dynamic aberrations.

TABLE VIII
ABERRATION CORRECTION COMPARISON IN RMS OF MIXING FREQUENCIES

Frequency / Hz	Before Correction / μm	After Correction / μm	Residual
0.025/0.1/0.25	0.225	0.080	35.7%
0.025/0.05/0.25	0.195	0.071	36.4%
0.01/0.025/0.05	0.168	0.061	36.1%

TABLE IX
ABERRATION CORRECTION COMPARISON IN PV OF MIXING FREQUENCIES

Frequency / Hz	Before Correction / μm	After Correction / μm	Residual
0.025/0.1/0.25	0.905	0.608	67.2%
0.025/0.05/0.25	0.805	0.543	67.5%
0.01/0.025/0.05	0.817	0.448	54.8%

V. CONCLUSION

In this paper, dynamic characteristics of aberrations from different sources during operation of solar telescopes are analyzed. For low spatio-temporal frequency aberrations caused by structure's deflection and thermal deformation, oblique and defocusing aberrations are majority and can be effectively reduced to 0.05λ by secondary mirror movement. For aberrations caused by atmospheric turbulence and wind load with high dynamic frequency, it is necessary to divide the actual wavefront data based on frequencies and correct the low frequency components. The relationship between the secondary mirror adjustment frequency and effectiveness of dynamic aberration correction is studied. Numerical simulation results show that given the correction frequency of secondary mirror adjustment is 10 times higher than aberration frequency, the average aberration RMS and PV after correction are 70% and 40%lower than before, and this frequency ratio is taken as the benchmark of spatio-temporal frequency division in this paper.

Experiments were conducted with adjustment frequency and aberration frequency of 0.5 Hz and 0.05 Hz respectively. The effectiveness of correction is proven with average aberration RMS and PV after correction 53% and 62% of before. Finally, secondary mirror adjustment on mixed dynamic aberration is proved by simulation and experiment. After spatiotemporal frequency separation, the secondary mirror adjustment can effectively reduce the overall RMS of dynamic aberrations containing high frequency components. After correction, the average RMS and PV of mixed aberrations of each group are lower than 40% and 70% of before. Compared with active optics system of LSST

[3], our system correction frequency is about 20 times higher. It allows the POST telescope response faster to aberrations and environmental challenges. The method of secondary mirror rigid body displacement correction can effectively reduce the low spatio-temporal frequency aberrations during the operation of solar telescope system without additional optical component, which processes good development prospect and application value.

Reference

[1] N. Gu, C. Li, Y. Cheng, and C. Rao, "Thermal control for light-weighted primary mirrors of large ground-based solar telescopes," *Proc. SPIE*, vol. 5, no. 1, 2019, Art. no. 014005, doi: 10.1117/1.JATIS.5.1.014005.

[2] N. Gu et al., "Passive control of the temperature homogeneity for the primary mirror surface of large ground based solar telescopes," *Proc. SPIE*, vol. 5, no. 4, 2019, Art. no. 044007, doi: 10.1117/1.JATIS.5.4.044007.

[3] Y. Cao et al., "The active correction of offset error of large aperture ground based telescopes based on hexapod platform," *Opt. Precis. Eng.*, vol. 11, pp. 2452–2465, 2020.

[4] A. Rakish, "Using a laser tracker for active alignment on the large binocular telescope," *Proc. SPIE*, vol. 8444, 2012, Art. no. 844454.

[5] D. Neill et al., "Overview of LSST active optics system," *Proc. SPIE*, vol. 9150, 2014, Art. no. 91500G.

[6] W. Schmidt et al., "The 1.5 meter solar telescope GREGOR," *Astronomische Machrichten*, vol. 333, no. 9, pp. 796–809, 2012.

[7] W. Cao et al., "Scientific instrumentation for the 1.6m new solar telescope in big bear," *Astronomische Machrichten*, vol. 331, no. 6, pp. 636–639, 2010.

[8] R. Upton, "Optical control of the advanced technology solar telescope," *Appl. Opt.*, vol. 45, no. 23, pp. 5881–5896, 2006.

[9] K. Wang, Y. Dai, and Z. Jin, "Attitude alignment method of solar telescope secondary mirror based on aberration detection," *Acta Photonica Sinica*, vol. 51, no. 6, Jun. 2022.

[10] C. Rao et al., "POST- prototype for the Chinese large solar telescope," *Proc. SPIE*, vol. 5, no. 2, 2019, Art. no. 024004.

[11] C. Rao et al., "First light of the 1.8-m solar telescope – CLST," *Sci. China Phys., Mech. Astron.*, vol. 63, no. 10, 2020, Art. no. 109631.

[12] D. Ren, T. Zhang, and G. Wang, "An optimized high-performance technique for adaptive optics static aberration correction," *Opto-Electron. Eng.*, vol. 49, no. 3, 2022, Art. no. 210319, doi: 10.12086/oee.2022.210319.

[13] Y. Guo et al., "Adaptive optics based on machine learning: A review," *Opto-Electron. Adv.*, vol. 5, no. 7, 2022, Art. no. 200082, doi: 10.29026/oea.2022.200082.

[14] K. Thompson, "Description of the third-order optical aberrations of near-circular pupil optical systems without symmetry," *J. Opt. Soc. Amer. Opt. Image Sci. Vis.*, vol. 22, no. 7, pp. 1389–1401, 2005.

[15] S. Zhao et al., "Research on low spatio-temporal frequency wavefront aberration correction technology of solar telescope," *Infrared Laser Eng.*, vol. 52, no. 7, pp. 1389–1401, 2023.

[16] Z. Gu et al., "Application of modified sensitivity matrix method in alignment of off-axis telescope," *Opt. Precis. Eng.*, vol. 23, no. 9, p. 10, 2015.

[17] Y. Cao and W. Ma, "Application of two step sensitivity matrix method in Cassegrain telescope alignment," *Opto-Electron. Eng.*, vol. 47, no. 2, 2020, Art. no. 180536.

[18] Y. Zhang, C. Rao, and X. Li, *Adaptive Optics and Laser Control*. Arlington, Virginia: National Defence Industry Press.

[19] X. Li, "Optimization of modal reconstruction algorithm and control algorithm in adaptive optics system," Ph.D. dissertation, Inst. Optics Electron., Chin. Acad. Sci., Changchun, China, 2000.

[20] X. Li, "Research on secondary mirror's correction technology for the misaligned wave aberration of large aperture space remote sensor," Ph.D. dissertation, Changchun Inst. Opt., Fine Mech. Phys., Chin. Acad. Sci., Changchun, China, 2020.

[21] T. Wu and H. Hua, *Mechanical Vibrations*. Beijing, China: Tsinghua Univ. Press, 2014.

[22] Z. Zhang and Y. Feng, "DS-TWR ranging method based on adaptive Kalman filter," *Ind. Control Comput.*, vol. 36, no. 2, pp. 86–88, 2023.

[23] Y. Yang, L. Huang, Y. Xiao, and N. Gu, "Polarized Shack-Hartmann wavefront sensor," *Front. Phys.*, vol. 11, 2023, Art. no. 1091848, doi: 10.3389/fphy.2023.1091848.